

# Femtosecond time-resolved dynamical Franz-Keldysh effect

T. Otake<sup>1</sup>, Y. Shinohara<sup>2</sup>, S. A. Sato<sup>3</sup>, and K. Yabana<sup>1,3,4</sup>

<sup>1</sup>*Kansai Photon Science Institute, Japan Atomic Energy Agency, Kizugawa, Kyoto 619-0615, Japan*

<sup>2</sup>*Max-Planck Institut für Mikrostrukturphysik, Weinberg 2, D-06120, Halle, Germany*

<sup>3</sup>*Graduate School of Pure and Applied Sciences, University of Tsukuba, Tsukuba 305-8571, Japan*

<sup>4</sup>*Center for Computational Sciences, University of Tsukuba, Tsukuba 305-8577, Japan*

We theoretically investigate the dynamical Franz-Keldysh effect in femtosecond time resolution, that is, the time-dependent modulation of a dielectric function at around the band gap under an irradiation of an intense laser field. We develop a pump-probe formalism in two distinct approaches: first-principles simulation based on real-time time-dependent density functional theory and analytic consideration of a simple two-band model. We find that, while time-average modulation may be reasonably described by the static Franz-Keldysh theory, a remarkable phase shift is found to appear between the dielectric response and the applied electric field.

In last two decades, intense coherent light of different characteristics have become available owing to advances in laser sciences and technologies. Ultrashort laser pulses can be as short as a few tens of attosecond, forming a new field of attosecond science [1]. Intense laser pulses of mid-infrared (MIR) or THz frequencies have also become available recently [2, 3]. Employing these extreme sources of coherent light, it is possible to investigate the optical response of materials in real time with a resolution much less than an optical cycle [1, 4–8].

The dielectric function  $\epsilon(\omega)$  is the most fundamental quantity characterizing the optical properties of matter. Modulation of the dielectric function in the presence of electromagnetic fields have been a subject of investigation for many years. The change under a static electric field is known as the Franz-Keldysh effect (FKE) [9–16], and that under an alternating electric field is known as the dynamical FKE (DFKE) [17–22]. An important parameter which distinguishes DFKE from the static FKE is the adiabaticity parameter  $\gamma = U_p/\Omega$ , where  $U_p = e^2 E^2 / 4\mu\Omega^2$  is the ponderomotive energy, and  $\Omega$  is the frequency of the field,  $\mu$  is the reduced mass of the electron, and  $E$  is the electric field [19]. A multi-photon picture applies for  $\gamma \ll 1$ , and a static FKE picture is appropriate for  $\gamma \gg 1$ . Laser pulses having  $\gamma \sim 1$  is an intriguing regime where novel and unobvious DFKE phenomena are expected.

In previous investigations of DFKE, the main focus was on the modulation of the optical response averaged over times much longer than the optical cycle, examining the time-averaged fine structure [18] and shifts in excitation structures [19]. In the present Letter, we examine DFKE in time domain, with a resolution much less than the cycle of the applied optical field. The DFKE response in subfemtosecond time resolution is very relevant to ultrafast optical switching in the terahertz or even petahertz ( $10^{15}$  hertz) domain [5, 7]. A first experimental report on the DFKE with a femtosecond time resolution has recently been given by Novelli *et al.* [7] for GaAs, employing an intense pump pulse of THz frequency. They observed an interesting time shift between

the pump pulse and the modulation of dielectric function, but the mechanism of the observed time profile was not understood. To uncover the physics of time-resolved DFKE, we develop a pump-probe formalism in two different theoretical approaches: first-principles numerical simulations based on time-dependent density functional theory (TDDFT [25]) and analytic investigation for a two-band model. Combining two approaches, we can understand not only the strength of the modulation but the phase with respect to the pump field as well.

In real-time TDDFT, we describe electron dynamics in a unit cell of a crystalline solid under a spatially-uniform electric field  $E(t)$ . The method has been applied for calculations of linear optical responses [26] and nonlinear electronic excitations by intense laser pulses [27–33]. Treating the field by a vector potential  $\vec{A}(t) = -c \int^t dt' \vec{E}(t')$ , the electron dynamics is described by the following time-dependent Kohn-Sham (TDKS) equation:

$$i \frac{\partial}{\partial t} \psi_i(\vec{r}, t) = \left[ \frac{1}{2m} \left( \vec{p} + \frac{e}{c} \vec{A}(t) \right)^2 + V(\vec{r}, t) \right] \psi_i(\vec{r}, t). \quad (1)$$

where  $m$  is the electron mass and  $V(\vec{r}, t)$  is composed of electron-ion, electron-electron Hartree, and exchange-correlation potentials. We use a norm-conserving pseudopotential for the electron-ion potential [34, 35]. For the exchange-correlation potential, we employ an adiabatic local density approximation, using the same functional form of the potential for both ground state and time evolution calculations [36]. We calculate electron dynamics in diamond, using a cubic unit cell containing eight carbon atoms. The TDKS equation is solved in real time and real space. The real-space grids of  $22^3$  is used for the unit cell, and  $32^3$  grids for the  $k$ -points. The Taylor expansion method is used for the time evolution [37] with a time step of  $\Delta t = 0.02$  in atomic unit. The number of time steps is typically 70,000.

An important output of the calculation is the average electric current density as a function of time. It is given

by

$$J(t) = -\frac{e}{mV} \int_V d\vec{r} \sum_i \text{Re} \psi_i^* \left( \vec{p} + \frac{e}{c} \vec{A}(t) \right) \psi_i + J_{NL}(t), \quad (2)$$

where  $V$  is a volume of the unit cell.  $J_{NL}(t)$  is the current caused by non-locality of the pseudopotential.

It should be mentioned that  $\vec{A}(t)$  in the TDKS equation (1) is the vector potential in the medium and not that of the incidence pulse in the vacuum. As we discussed in [38], the relation between the two depends on the macroscopic shape of the materials as well as the direction of the polarization. Exchange-correlation effects may also appear in the vector potential in time-dependent current density functional theory [39], which we ignore for simplicity.

To examine the DFKE, we carry out simulations solving the TDKS equation (1) including both pump and probe electric fields in the vector potential  $\vec{A}(t)$  [32]. We assume that both pump and probe electric fields are linearly polarized and are orthogonal to each other. We denote the pump electric field as  $E_P(t)$  and the probe electric field as  $E_p(t)$ . The probe electric field is assumed to be weak enough to be treated by the linear response theory. We denote the electric current caused by the probe field as  $J_p(t)$ . They are related by the time-domain conductivity  $\sigma(t, t')$  as

$$J_p(t) = \int_{-\infty}^t dt' \sigma(t, t') E_p(t'). \quad (3)$$

We note that the conductivity  $\sigma(t, t')$  depends on both times  $t$  and  $t'$  rather than just time difference  $t - t'$  due to the presence of the pump pulse.

We derive a frequency-dependent conductivity at time  $T$  from the conductivity  $\sigma(t, t')$ . We first note that, in the absence of the pump electric field, the frequency-dependent conductivity  $\tilde{\sigma}(\omega)$  is related to the Fourier transforms of the electric field and the induced current as,  $\tilde{\sigma}(\omega) = \int dt e^{i\omega t} J_p(t) / \int dt e^{i\omega t} E_p(t)$ . This is derived from Eq. (3) noting  $t - t'$  dependence of the conductivity. We employ this relation in the presence of the strong pump field. To introduce the time  $T$  to explore the response, a pulsed electric field is employed for  $E_p(t)$  whose envelope shows a maximum at  $t = T$ . Thus, in this consideration, the probe electric field has a dual role, to specify the time  $T$  at which we explore the response of the medium and to distort the medium to examine responses of the system. We consider that this dual role of the probe pulse will be adopted to measure the transient dielectric functions in most experiments.

In practice, we use the following electric fields. The pump field is of the form  $E_P(t) = E_{0,P} f(t) \sin \Omega t$  with the central angular frequency  $\Omega$  set to  $\Omega = 0.4$  eV; its direction is along the [001] axis. The field is turned on adiabatically by  $f(t)$ , given by  $f(t) = \sin^2\left(\frac{\pi}{2T_P} t\right)$  for  $0 < t < T_P$  and  $f(t) = 1$  for  $t \geq T_P$  and  $T_P = 10$  fs.

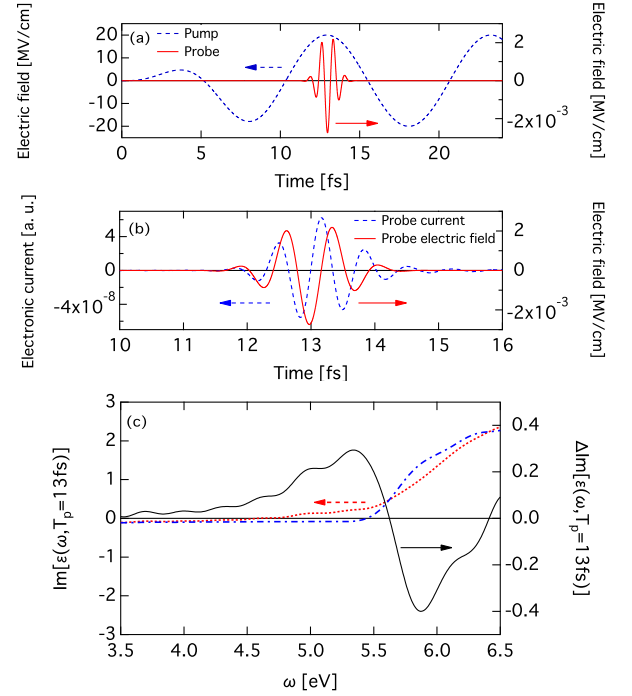


FIG. 1. (a) Pump (blue-dashed line) and probe (red-solid line) electric fields are shown. (b) The electronic current (blue-dashed line) induced by the probe electric field (red-solid line). (c) The imaginary part of the dielectric function in the presence of the pump field,  $\text{Im}[\epsilon(\omega, T_p = 13 \text{ fs})]$  (red-dashed line), and in the absence of the pump field,  $\text{Im}[\epsilon(\omega)]$  (blue-dash-dot line). Black-solid line shows the difference,  $\text{Im}[\epsilon(\omega, T_p = 13 \text{ fs})] - \text{Im}[\epsilon(\omega)]$ .

The probe field is of the form  $E_p(t) = E_{0,p} \sin(\omega_p t) \exp(-(t - T_p)^2/\eta^2)$ , oriented in the [100] direction. The average frequency  $\omega_p$  is set to 5.6 eV, which is equal to the calculated band gap energy of diamond in LDA. The field strength is set to  $E_{0,p} = 2.7 \times 10^{-3}$  MV/cm, which is small enough to probe the linear response of the medium. The pulse duration  $\eta$  is set to  $\eta = 0.7$  fs. With such a short duration, we may scan the spectrum of broad frequency region around the band gap from a single pump-probe calculation.

The frequency-dependent conductivity is calculated as the ratio of the Fourier-transformed current  $J_p(t)$  and field  $E_p(t)$  as

$$\tilde{\sigma}(T_p, \omega) = \frac{\int dt e^{i\omega t} g(t - T_p) J_p(t)}{\int dt e^{i\omega t} E_p(t)}, \quad (4)$$

where  $g(t)$  is a filter function to suppress spurious oscillations arise from the numerical cutoff in the integration.

Figure 1 shows an example of our pump-probe calculations. In (a), the blue-dashed line shows the electric fields of the pump field  $E_P(t)$ , and the red-solid line shows the electric field of the probe pulse  $E_p(t)$ . The magnitude of

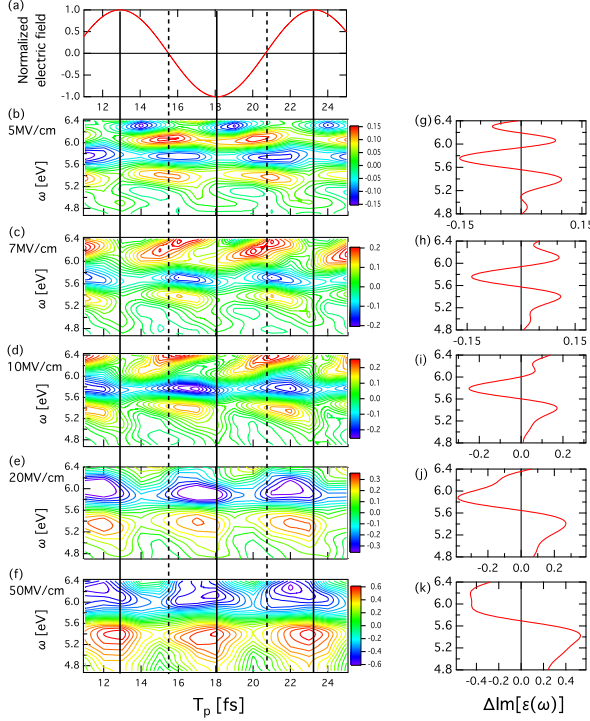


FIG. 2. Contour plots (left) and their time averages (right) of  $\Delta\text{Im}[\epsilon(\omega, T_p)]$  under the MIR pump field of the intensity of (b,g) 5, (c,h) 7, (d,i) 10, (e,j) 20, and (f,k) 50 MV/cm. The time dependence of the pump electric field is shown in (a). In panels (a)-(f), the vertical solid (dashed) lines indicate the time of maximum (zero) of the pump electric field.

the pump electric field,  $E_{0,P}$ , is set to 20 MV/cm. The probe pulse is applied at a time when the magnitude of the pump field is maximum. The electric current induced by the probe pulse,  $J_p(t)$ , is shown by the blue-dashed line in (b). The conductivity is calculated from the probe current using Eq. (4), and then converted to the dielectric function using a formula  $\epsilon = 1 + 4\pi i\sigma/\omega$ , which is valid in the presence of the strong pump field. The imaginary part of the dielectric function,  $\text{Im}[\epsilon(\omega, T_p = 13\text{fs})]$ , is shown in (c). The red-dotted and blue dot-dashed lines present the dielectric function with and without the pump field, respectively. A change of the imaginary part of the dielectric function,  $\Delta\text{Im}[\epsilon(\omega, T_p = 13\text{fs})]$ , is shown by the black-solid line. It indicates modulations of an exponential tail below and an oscillation above the band gap ( $\omega = 5.5\text{ eV}$ ). This behavior may be understood by the static FKE.

Figure 2 shows changes of the imaginary part of the dielectric function caused by the strong pump field,  $\Delta\text{Im}[\epsilon(\omega, T_p)] = \text{Im}[\epsilon(\omega, T_p)] - \text{Im}[\epsilon(\omega)]$ . In (a), time profile of the pump electric field is shown. In (b) - (f), changes of imaginary part of the dielectric function are shown in contour plots for four intensities. Horizontal axis is the time  $T_p$  and the vertical axis is the frequency  $\omega$ . In (g)-(k), modulations averaged over time are shown

as a function of frequency.

We first look at the case of strongest pump electric field,  $E_{0,P} = 50\text{ MV/cm}$ , shown in (f) and (k). We find that an increase of the absorption below and a decrease above the band gap are seen when the magnitude of the pump electric field is close to the maximum. The modulation is small when the electric field is close to zero. This fact indicates the static FKE appears instantaneously following the change of the pump field. We confirmed the modulation is well fitted by the static FKE formula if we assume the effective mass of  $\mu = 0.25m$ . With this value of the effective mass, the adiabatic parameter  $\gamma$  is 29.5, much larger than unity, which is consistent with the appearance of the static FKE.

As the field intensity decreases, we find changes in two aspects, one along the frequency (vertical) axis and the other along the time (horizontal) axis. Above the band gap, we find an oscillatory behavior in the frequency (vertical) direction. This is clearly seen in the time-average behaviors shown in (g)-(k). For example, at the electric field of 10 MV/cm shown in (d) and (i), the modulation is negative between 5.6 eV (band gap) to 6.0 eV. It then becomes positive above 6.0 eV.

Along the time (horizontal) axis, we can see a striking change in the phase between the modulation and the pump electric field. At the strongest electric field (f), the modulation and the pump electric field is in phase, as mentioned above. As the intensity of the pump field decreases, a phase shift forward in time is seen. The amount of the phase difference increases as the magnitude of the pump field decreases, as seen from (b) to (f). At the lowest intensity (b), the modulation signals appear at times when the pump field is close to zero. The parameter  $\gamma$  for these intensities are (b) 0.29, (c) 0.58, (d) 1.19, and (e) 4.76. Thus the phase change becomes appreciable when the  $\gamma$  value is around and below unity.

To understand behaviors of the DFKE signals seen in the numerical simulation, we develop analytic consideration. In the following, we consider a system described by a time-dependent Schrödinger equation in place of the TDKS equation (1),  $i(\partial/\partial t)\psi_i = [(\vec{p} + e\vec{A}(t)/c)^2/2m]\psi_i + V\psi_i$  where  $V$  is a time-independent, lattice periodic potential. We assume that the solution is well approximated by the so-called Houston function [17, 40]. The Houston function is expressed using static Bloch orbitals  $u_{n,\vec{k}}(\vec{r})$  and orbital energies  $\epsilon_{n,\vec{k}}$  as

$$w_{n,\vec{k}}(\vec{r}, t) = u_{n,\vec{k}+e\vec{A}(t)/c}(\vec{r}) \exp\left[-i \int^t \epsilon_{n,\vec{k}+e\vec{A}(t')/c} dt'\right]. \quad (5)$$

We may construct an analytic expression for the conductivity  $\sigma(t, t')$  of (4) as given in the supplementary material. We further assume a two band model composed of occupied valence ( $v$ ) and unoccupied conduction ( $c$ ) bands. The electron-hole excitation energy is assumed to be parabolic,  $\epsilon_{c\vec{k}} - \epsilon_{v\vec{k}} = \epsilon_g + \vec{k}^2/2\mu$ , where  $\epsilon_g$  is the

band gap energy and  $\mu$  is the reduced mass of the electron and the hole. We also assume that matrix elements of a momentum operator is independent of crystalline momentum,  $\langle u_{v\vec{k}} | -i\vec{\nabla} | u_{c\vec{k}} \rangle = \vec{p}_{vc}$ .

We first consider a conductivity under a static electric field  $E$ . In this case, the conductivity in time domain depends on the time difference  $t - t'$ . Under assumptions described above, we obtain a modulation of the conductivity which coincides with an ordinary result of the static FKE,

$$\text{Re}\sigma(\omega) = \frac{(2\mu)^{3/2}}{2\omega} |p_{vc}|^2 \sqrt{\theta} \{ -X A_i^2(X) + A_i'^2(X) \}, \quad (6)$$

where  $X = (\epsilon_g - \omega)/\theta$ ,  $\theta = (E^2/2\mu)^{1/3}$ , and  $A_i(x)$  is the Airy function.

We now move to the case of time-dependent pump field given by  $A_P(t) = A_0 \cos \Omega t$ . For the periodic pump field, the conductivity  $\sigma(t, t')$  has also a periodicity,  $\sigma(t, t') = \sigma(t - 2\pi/\Omega, t' - 2\pi/\Omega)$ . Then the real part of the conductivity  $\tilde{\sigma}(T, \omega)$  defined by Eq. (4) (with  $g(t) = 1$ ) can be Fourier expanded as

$$\text{Re}\sigma(T, \omega) = \sum_m C_m(\omega) \cos 2m\Omega T + S_m(\omega) \sin 2m\Omega T. \quad (7)$$

For simplicity, we employ an instantaneous probe field,  $E_p(t) = k\delta(t - T)$ , in Eq. (4). Then, in the two-band model,  $C_m(\omega)$  and  $S_m(\omega)$  are given by

$$C_m(\omega) = \frac{\mu^{3/2} |p_{vc}|^2}{\sqrt{2\pi}} \sum_l \left[ \frac{\sqrt{\epsilon_k^+} \xi_{l,2m}(k^+)}{\omega + 2m\Omega} - \frac{\sqrt{\epsilon_k^-} \xi_{l,2m}(k^-)}{\omega - 2m\Omega} \right] \quad (8)$$

$$S_m(\omega) = -\frac{\mu^{3/2} |p_{vc}|^2}{\sqrt{2\pi^2}} \int_0^\infty d\epsilon_k \sqrt{\epsilon_k} \sum_l \xi_{l,2m}(k) \times \left[ \frac{1}{(\omega + 2m\Omega) \{ \omega - (\epsilon_k + \epsilon_g + U_p) - (l - 2m)\Omega \}} + \frac{1}{(\omega - 2m\Omega) \{ \omega + (\epsilon_k + \epsilon_g + U_p) + (l - 2m)\Omega \}} \right], \quad (9)$$

where  $\xi_{l,n}(k) = \int_{-1}^1 d\cos\theta_k J_l(\theta_1, \theta_2) J_{l-n}(\theta_1, \theta_2)$  with  $J_l(\theta_1, \theta_2) = \sum_m J_{l-2m}(\theta_1) J_m(\theta_2)$ ,  $J_l(x)$  is the Bessel function.  $\theta_1, \theta_2, U_p$  are given by  $\theta_1 = eA_0 \cos\theta_k / \mu c \Omega$ ,  $\theta_2 = e^2 A_0^2 / 8\mu c^2 \Omega$ , and  $U_p = e^2 A_0^2 / 4\mu c^2$ .  $k^\pm$  and  $\epsilon_k^\pm$  are defined by  $k^\pm = \sqrt{2\mu\epsilon^\pm}$  and  $\epsilon_k^\pm = \pm\omega - (\epsilon_g + U_p) - (l - 2m)\Omega$ . The derivation of this expression is given in the supplementary material. We note that the terms with  $m = \pm 1$  are responsible for the phase shift seen in Fig. 2.

We numerically calculate the change of the dielectric function  $\Delta\text{Im}[\epsilon(\omega, T_p)]$  using Eqs. (7) - (9). Figure 3 (a)-(d) show the contour plot where the horizontal axis is the phase defined by  $\Omega T_p$ . In Fig. 3 (e)-(h), modulations averaged over time is shown by red-solid lines.

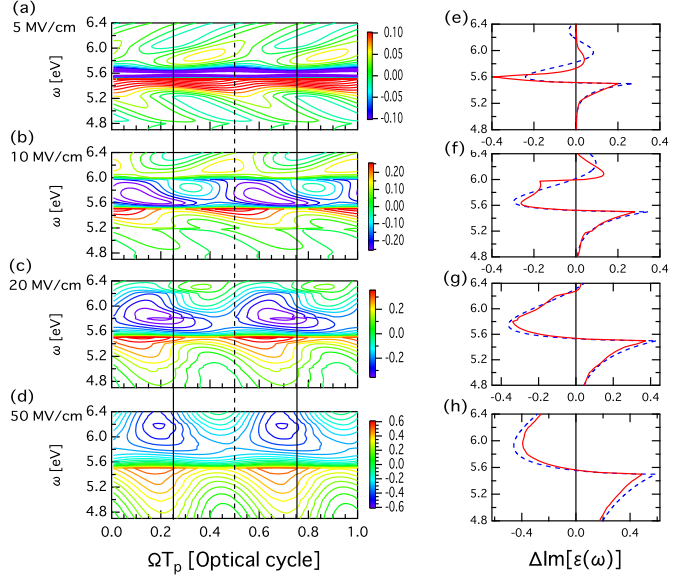


FIG. 3. Contour plots and time averages of  $\Delta\text{Im}[\epsilon(\omega, T_p)]$  in the two-band model for the pump field intensities of (a,e)  $E_0 = 5$ , (b,f) 10, (c,g) 20, and (d,h) 50 MV/cm. In the left panels (a)-(d), the horizon axis is the phase defined by  $\Omega T_p$ . The vertical solid (dashed) lines indicate the position of maximum (minimum) of the electric field. In the right panels (e)-(h), red-solid lines is the time average of the modulation. Blue-dotted lines show result of static FKE.

Blue-dashed lines show results of static FKE: the time-averaged modulation using static formula (6) where the parameter  $\theta$  is evaluated using time-dependent electric field,  $E(t)$ . The parameters in the two-band model are set to reproduce responses in the TDDFT calculations: The frequency of pump field is set to  $\Omega = 0.4$  eV, the reduced mass is set to  $\mu = 0.25$ , and the dipole matrix element is set to  $|p_{cv}|^2 = 0.928$  in atomic unit.

We first look at time-averaged modulations shown in panels (e)-(h). In all panels, we find appearances of absorption below the band gap and decrease above the band gap. They show a similar behavior to Fig. 2 (g)-(k). We also find that the time-averaged modulation is quite close to the estimation by the static FKE, even at the smallest intensity where the  $\gamma$  value is much less than unity.

We next look at the time dependence of the modulation. At the strong pump electric field (d), we find a large modulation when the magnitude of the pump electric field is large. We find a phase shift as the pump electric field decreases. The maximum of the modulation moves forward in time. From these observations, we can say that all the features seen in the first-principles TDDFT calculations shown in Fig. 2 are reproduced by the analytic formula of Eqs. (7) - (9) of the simple two-band model.

In summary, we developed a theoretical pump-probe formalism to investigate the dynamical Franz-Keldysh



effect in time-domain, in femtosecond time resolution much shorter than the optical cycle of the applied pump field. Both numerical simulations based on real-time time-dependent density functional theory and an analytic approach in the two-band model reveals the same behavior for the modulations of dielectric properties. We find the time-averaged behavior in the DFKE can be well described by the static FKE. The most remarkable feature of the DFKE is that there appears a phase shift between the modulation of the dielectric function and the applied pump field which becomes significant as the magnitude of the electric field decreases.

The authors thank G.F. Bartsch for discussions and for carefully reading manuscript. This work is supported by a Grant-in-Aid for Scientific Research (No. 21740303). Numerical calculations were performed on the supercomputer PRIMARGY BX900 at the Japan Atomic Energy Agency (JAEA) and the K computer at the RIKEN Advanced Institute for Computational Science (proposal number hp120065).

- 
- [1] M. Hentschel, R. Klenberger, Ch. Spielmann, G.A. Reider, N. Milosevic, T. Brabec, U. Heinzmann, M. Drescher, and F. Krausz, *Nature* **414**, 509 (2001).
  - [2] H. Hirori, A. Doi, F. Blanchard, and K. Tanaka, *App. Phys. Lett.* **98**, 091106 (2011).
  - [3] A.H. Chin, O.G. Calderón, and J. Kono, *Phys.Rev. Lett.* **86**, 3292 (2001).
  - [4] H.Hirori, K. Shinokita, M. Shirai, S. Tani, Y. Kadoya, and K. Tanaka, *Nat. Comm.* **2**, 594 (2011).
  - [5] A. Schiffrin, T. Paasch-Colberg, N. Karpowicz, V. Apalkov, D. Gerster, S. Mühlbrandt, M. Korbman, J. Reichert, M. Schultze, S. Holzner, J.V. Barth, R. Kienberger, R. Ernstorfer, V.S. Yakovlev, M.I. Stockman, and F. Krausz, *Nature* **493**, 70 (2013).
  - [6] M. Schultze, E.M. Botschafter, A. Sommer, S. Holzner, W. Schweinberger, M. Fless, M. Hofstetter, R. Kienberger, V. Apalkov, V.S. Yakovlev, M.I. Stockman, F. Krausz, *Nature* **493**, 75 (2013).
  - [7] F. Nobelli, D. Fausti, F. Giusti, F. Parmigiani, and M. Hoffmann, *Scientific Reports* **3** 1227 (2013).
  - [8] M. Schultze, K. Ramasesha, C.D. Pemmaraju, S.A. Sato, D. Whitmore, A. Gandman, J.S. Prell, L.J. Borja, D. Prendergast, K. Yabana, D.M. Neumark, S.R. Leone, *Science* **346**, 1348 (2014).
  - [9] W.Franz, *Z. Naturforsch. Teil A* **13**, 484 (1958).
  - [10] L. V. Keldysh, *Sov. Phys. JETP* **34**, 788 (1958).
  - [11] K. Tharmalingam, *Phys. Rev.* **130**, 2204 (1963).
  - [12] B. O. Seraphin and R. B. Hess, *Phys. Rev. Lett.* **14**, 138 (1965).
  - [13] R. E. Nahory and J. L. Shay, *Phys. Rev. Lett.* **21**, 1569 (1968).
  - [14] H.Shen, M. Dutta, *J. Appl. Phys.* **78**, 2151 (1995).
  - [15] J.K. Wahlstrand, J.E. Sipe, *Phys. Rev. B* **82**, 075206 (2010).
  - [16] F. Duque-Gomez, J.E. Sipe, *J. Phys. Chem. Solids* **76**, 138 (2015).
  - [17] Y. Yacoby, *Phys. Rev.* **169**, 610 (1968).
  - [18] A. P. Jauho and K. Johnsen, *Phys.Rev. Lett.* **76**, 4576 (1996).
  - [19] K. B. Nordstrom, K. Johnsen, S. J. Allen, A.-P. Jauho, B. Birnir, J. Kono, T. Noda, H. Akiyama, and H. Sakaki, *Phys. Rev. Lett.* **81**, 457 (1998).
  - [20] Ajit Srivastava, Rahul Srivastava, Jigang Wang, and Junichiro Kono, *Phys.Rev.Lett.* **93**, 157401 (2004).
  - [21] Y. Mizumoto, Y. Kayanuma, A. Srivasatava, J. Kono, and A. H. Chin, *Phys. Rev. B* **74**, 045216 (2006).
  - [22] S. Ghimire, A.D. DiChiara, E. Sistrunk, U.B. Szafruga, *Phys. Rev. Lett.* **107**, 167407 (2011).
  - [23] A. H. Chin, J. M. Bakker, and J. Kono, *Phys. Rev. Lett.* **85**, 3293 (2000).
  - [24] Ajit Srivastava, Rahul Srivastava, Jigang Wang, and Junichiro Kono, *Phys. Rev. Lett.* **93**, 157401 (2004).
  - [25] E. Runge and E. K. U. Gross, *Phys.Rev. Lett.* **52**, 997 (1984).
  - [26] G.F. Bertsch, J.-I. Iwata, A. Rubio, and K. Yabana, *Phys. Rev. B* **62**, 7998 (2000).
  - [27] T. Otobe, M. Yamagiwa, J. -I. Iwata, K. Yabana, T. Nakatsukasa, and G. F. Bertsch, *Phys. Rev. B* **77**, 165104 (2008).
  - [28] T. Otobe, K. Yabana, J.-I. Iwata, *J. Phys.: Condens. Matter.* **21**, 064224 (2009).
  - [29] Y. Shinohara, K. Yabana, Y. Kawashita, J.-I. Iwata, T. Otobe, and George F. Bertsch, *Phys. Rev. B* **82**, 155110 (2010).
  - [30] Y. Shinohara, S. A. Sato, K. Yabana, J.-I. Iwata, and T. Otobe, *J. Chem. Phys.* **137** 22A527 (2012).
  - [31] T. Otobe, *J. Appl. Phys.* **111**, 093112 (2012).
  - [32] S.A. Sato, K. Yabana, Y. Shinohara, T. Otobe, G.F. Bertsch, *Phys. Rev.* **B89**, 064304 (2014).
  - [33] G. Wachter, C. Lemell, J. Burgdorfer, S.A. Sato, X.M. Tong, K. Yabana, *Phys. Rev. Lett.* **113**, 087401 (2014).
  - [34] N. Troullier and J.L. Martins, *Phys. Rev.* **B43**, 1993 (1991).
  - [35] L. Kleinman and D. M. Bylander, *Phys. Rev. Lett.* **48**, 1425 (1982).
  - [36] J. P. Perdew and A. Zunger, *Phys. Rev. B* **23**, 5048 (1981).
  - [37] K. Yabana and G.F. Bertsch, *Phys. Rev.* **B54**, 4484 (1996).
  - [38] K. Yabana, T. Sugiyama, Y. Shinohara, T. Otobe, and G. F. Bertsch, *Phys. Rev. B* **85**, 045134 (2012).
  - [39] G. Vignale and W. Kohn, *Phys. Rev. Lett.* **77**, 2037 (1996).
  - [40] W. V. Houston, *Phys. Rev.* **51**, 184 (1940).